0026-895X/09/7501-183–195$20.00
MOLECULAR PHARMACOLOGY
Copyright © 2009 The American Society for Pharmacology and Experimental Therapeutics
Mol Pharmacol 75:183–195, 2009

Vol. 75, No. 1
51490/3418828
Printed in U.S.A.

Amitriptyline Activates Cardiac Ryanodine Channels and Causes Spontaneous Sarcoplasmic Reticulum Calcium Release

Nagesh Chopra, Derek Laver, Sean S. Davies, and Björn C. Knollmann

Oates Institute for Experimental Therapeutics and Division of Clinical Pharmacology, Departments of Medicine and Pharmacology, Vanderbilt University Medical Center, Nashville, Tennessee (N.C., S.S.D., B.C.K.); and Department of Biomedical Sciences, University of Newcastle and HMRI, Callaghan, Australia (D.L.).

Received August 19, 2008; accepted October 8, 2008

ABSTRACT

Patients taking amitriptyline (AMT) have an increased risk of sudden cardiac death, yet the mechanism for AMT's proarrhythmic effects remains incompletely understood. Here, we hypothesize that AMT activates cardiac ryanodine channels (RyR2), causing premature Ca^{2+} release from the sarcoplasmic reticulum (SR), a mechanism identified by genetic studies as a cause of ventricular arrhythmias and sudden cardiac death. To test this hypothesis, we measured the effect of AMT on RyR2 channels from mice and sheep and on intact mouse cardiomyocytes loaded with the Ca^{2+} fluorescent indicator Fura-2 acetoxymethyl ester. AMT induced trains of long channel openings (bursts) with 60 to 90% of normal conductance in RyR2 channels incorporated in lipid bilayers. The [AMT], voltage, and open probability (P_o) dependencies of burst frequency and duration indicated that AMT binds primarily to open RyR2 channels. AMT also activated RyR2 channels isolated from transgenic mice lacking cardiac calsequestrin. Reducing RyR2 P_o by increasing cytoplasmic [Mg^{2+}] significantly inhibited the AMT effect on RyR2 channels. Consistent with the single RyR2 channel data, AMT increased the rate of spontaneous Ca^{2+} releases and decreased the SR Ca^{2+} content in intact cardiomyocytes. Intracellular [AMT] were approximately 5-fold higher than extracellular [AMT], explaining AMT's higher potency in cardiomyocytes at clinically relevant concentrations (0.5–3 μM) compared with its effect in lipid bilayers (5–10 μM). Increasing extracellular [Mg^{2+}] attenuated the effect of AMT in intact myocytes. We conclude that the heretofore unrecognized activation of RyR2 channels and increased SR Ca^{2+} leak may contribute to AMT's proarrhythmic and cardiotoxic effects, which may be counteracted by interventions that reduce RyR2 channel open probability.

Clinical use of tricyclic antidepressants (TCAs) is limited by their narrow therapeutic window, with significant cardiovascular toxicity (Thanacoody and Thomas, 2005), including sudden cardiac death (SCD) and myocardial depression (Pimentel and Trommer, 1994) reported in overdose cases. Even at therapeutic doses, TCAs, in particular AMT, increase the rate of SCD (Ray et al., 2004). Among the TCAs, AMT is the agent most commonly associated with SCD (32%) in cases of acute overdose (Crouch et al., 2004). The therapeutic plasma concentration of AMT in humans is 0.3 μM; acute toxicity starts at 1.5 μM and is well established at 3 μM (Hardman and Limbird, 2001). Even though AMT acts on many cardiac membrane receptors, ion channels, transporters, and intracellular proteins (Hardman and Limbird, 2001), which may contribute to the AMT's toxic effect on the heart, the cause of AMT-induced SCD remains incompletely understood (Heard et al., 2001). In particular, QT prolongation is not commonly seen during long-term TCA therapy. More-

This work was supported in part by National Institutes of Health grants HL88635 and HL71670 (to B.C.K.), by the American Heart Association Established Investigator Award 0840071N (to B.C.K.), by the Australian Research Council grant DP0557780 (to D.R.L.), by an infrastructure grant from NSW Health through Hunter Medical Research Institute (to D.R.L.) and by a Senior Brawn Fellowship from the University of Newcastle (to D.R.L.).

This work was presented in abstract form at the 2007 American Heart Association annual scientific meeting [Chopra N, Laver D, Watanabe H, Menon U, Stein CM, and Knollmann BC (2007) Amitriptyline activates cardiac ryanodine receptors independently of its action on cardiac calsequestrin—role for amitriptyline linked sudden cardiac death. *Circulation* **116:**II-84] and the 2008 Biophysics Society annual scientific meeting [Laver D, Chopra N, and Knollmann BC (2008) Mechanisms for amitriptyline activation of cardiac RyRs and SR Ca^{2+} release. *Biophys J* **94:**2120].

N.C. and D.L. contributed equally to this study.

Article, publication date, and citation information can be found at http://molpharm.aspetjournals.org.

doi:10.1124/mol.108.051490.

ABBREVIATIONS: TCA, tricyclic antidepressant; SCD, sudden cardiac death; AMT, amitriptyline; SR, sarcoplasmic reticulum; RyR2, cardiac SR Ca^{2+} release channels; Casq2, cardiac calsequestrin; TES, *N*-tris [hydroxymethyl]methyl-2-aminoethanesulfonic acid; BAPTA, 1,2-bis(2-aminophenoxy)ethane-*N*,*N*,*N*′,*N*′-tetraacetic acid; P_o, open probability; AM, acetoxymethyl ester; SCR, spontaneous Ca^{2+} release; LC/MS/MS, liquid chromatography/tandem mass spectrometry; IMP, imipramine; τ_o, open time; τ_c, closed time; *I*, current.

over, only 15% of overdose cases display QT prolongation (Vieweg and Wood, 2004), suggesting that other arrhythmia mechanisms are in play.

In cardiac muscle, sarcolemmal depolarization activates voltage-gated L-type Ca^{2+} channels in the T-tubules. The ensuing Ca^{2+} influx triggers Ca^{2+} release from the sarcoplasmic reticulum (SR) via ryanodine receptor Ca^{2+} release channels (RyR2), collectively referred to as "excitation-contraction" coupling. Sensitization of RyR2 channels causing spontaneous SR Ca^{2+} releases has been implicated as cause of delayed afterdepolarization that can trigger ventricular arrhythmia and sudden cardiac death in both genetic and acquired arrhythmia syndromes in absence of QT prolongation (Knollmann and Roden, 2008).

Thus, we hypothesized that AMT activates RyR2 channel complex causing spontaneous SR Ca^{2+} release and SR Ca^{2+} store depletion in ventricular myocytes. This would constitute a novel molecular mechanism that could help explain the proarrhythmic effects and myocardial depression associated with AMT use. To test this hypothesis, we examined the effects of AMT on the activity of single RyR2s in artificial lipid bilayers and on SR Ca^{2+} handling of isolated ventricular myocytes.

We found that AMT increases RyR2 channel activity in bilayers and causes spontaneous SR Ca^{2+}-release events and SR Ca^{2+} store depletion in intact myocytes at concentrations relevant in humans (0.5–3 μM). The mechanism of this heretofore unrecognized AMT's action on SR Ca^{2+} handling is a direct activation of the RyR2 complex (i.e., the ryanodine receptor and/or associated proteins excluding calsequestrin) by AMT. Mg^{2+} attenuated the effect of AMT, suggesting a possible mechanism for the beneficial effects of Mg^{2+} administration observed in patients with AMT-induced cardiotoxicity.

Materials and Methods

Animal Model. The use of animals in this study was in accordance with the guidelines set by the Animal Care and Use Committees of Georgetown and Vanderbilt Universities in USA, and University of Newcastle in Australia. A total of 37 age (2–4 months) and sex matched mice of C57/BL6 background strain were used for all the experiments. In addition, six mice with gene-targeted ablation of cardiac calsequestrin (Casq2) as described previously (Knollmann et al., 2006) and one sheep was used for the study.

Preparation of SR Vesicles for Lipid Bilayer Studies. All buffers contained the protease inhibitors leupeptin (1 μg/ml), pepstatin A (1 μg/ml), benzamidine (1 mM), and phenylmethylsulfonyl fluoride (0.5 mM). Hearts were excised from mice anesthetized with inhaled mixture of 100% O_2 and isoflurane (Minrad Inc., Bethlehem, PA). After surgical level of anesthesia was confirmed by tail pinching, the heart was removed, and the animal was killed by exsanguination. Then the heart was rinsed in ice-cold PBS before being snap-frozen in liquid nitrogen. Hearts were stored at −80°C until required. Five to six hearts were homogenized using a $P_o$lytron homogenizer (Kinematica, Littau-Lucerne, Switzerland) (30 s at high speed) in 5 ml of ice-cold homogenization buffer (10 mM imidazole, 0.5 mM dithiothreitol, 3 mM sodium azide, ad 290 mM sucrose, pH 6.9). The homogenate was centrifuged at 8000*g* for 20 min (14,000 rpm; TLA-110; Beckman Coulter, Fullerton, CA). The supernatant was retrieved and spun at 417,000*g* for 30 min (TLA-110 at 100,000 rpm). This pellet was resuspended in 3 ml of ice-cold homogenization buffer also containing 0.65 M KCl (KCl buffer) and incubated on ice for 30 min. The homogenate was spun at 3000*g* for 10 min (TLA-110 at 9000 rpm), supernatant recovered and spun at 417,000*g* for 30 min. The pellet was resuspended in ~50 μl of ice-cold KCl buffer with 10 strokes of a Teflon/glass homogenizer. Preparation was maintained at 4°C during use and stored at −80°C. SR vesicles (containing RyR_2) were also obtained from sheep hearts and were reconstituted into artificial lipid bilayers as described previously (Laver et al., 1995).

Single Channel Measurements. Lipid bilayers were formed from phosphatidylethanolamine and phosphatidylcholine [8:2 (w/w); Avanti Polar Lipids, Alabaster, AL] in *n*-decane (50 mg/ml; MP Biomedicals, Irvine, CA) across an aperture of 150 to 250 μm in diameter in a Delrin cup. During SR-vesicle incorporation, the *cis* (cytoplasmic) solution contained 250 mM Cs^+ (230 mM $CsCH_3O_3S$ and 20 mM CsCl), 1.0 mM $CaCl_2$ and 500 mM mannitol, whereas the *trans* (luminal) solution contained 50 mM Cs^+ (30 mM $CsCH_3O_3S$ mM and 20 mM $CsCl_2$), and 0.1 mM $CaCl_2$. The osmotic gradient across the membrane and the Ca^{2+} in the *cis* solution aided vesicle fusion with the bilayer. After detection of RyR2 in the bilayer, 2 mM ATP and BAPTA was added to the *cis* solution, bringing the free [Ca^{2+}] down to 0.1 μM (4.5 mM BAPTA) or 1 μM (2 mM BAPTA). In addition, the [$CsCH_3O_3S$] in the *trans* solution was increased to 230 mM (i.e., establishing 250 mM Cs^+ in both *cis* and *trans* baths) by means of aliquot addition of 4 M stock. AMT (Sigma) was added to the *cis* bath via aliquots of a 5 mM stock in milliQ water. The cesium salts were obtained from Aldrich Chemical Company (St. Louis, MO), mannitol was obtained from Ajax chemicals and $CaCl_2$ from BDH Chemicals. Solutions were pH-buffered with 10 mM TES (MP Biomedicals) and solutions were titrated to pH 7.4 using CsOH (optical grade, MP Biomedicals).

During experiments the composition of the *cis* solution was altered either by addition of aliquots of stock solutions or by local perfusion of the bath near the bilayer. Local perfusion was done by flowing solution from a tube (300 μm, ID) and located within 100 μm of the bilayer. Flow rates of ~1 μl/s produced total solution exchange at the bilayer in <1 s (Laver and Curtis, 1996).

Bilayer potential was controlled using an Axopatch 200B amplifier (Axon Instruments). Electrical potentials are expressed using standard physiological convention (i.e., cytoplasmic side relative to the luminal side at virtual ground). Single channel recordings were obtained using bilayer potential difference of +40 mV. The current signal was digitized at 5 kHz and low-pass filtered at 1 or 2 kHz with a Gaussian digital filter. Open probability (P_o) was measured by the 50% threshold detection method. Analysis was carried out using Channel2 software (P. W. Gage and M. Smith, Australian National University, Canberra, Australia). Unless otherwise stated, data are presented as mean ± S.E.M.

Dwell-time frequency histograms of channel openings were obtained from single-channel recordings and were displayed as probabilities (counts/total number of events). These were plotted using the "log-bin" method suggested by Sigworth and Sine (1987), which displays exponential values as peaked distributions centered around their exponential time constant.

Cardiomyocyte Isolation. Single ventricular myocytes were isolated by a modified collagenase/protease method as described previously (Knollmann et al., 2006). All chemicals, unless otherwise specified were obtained from Sigma. All the experiments were conducted in Tyrode's solution containing 134 mM NaCl, 5.4 mM KCl, 1 mM $MgCl_2$, 10 mM glucose, and 10 mM HEPES, pH adjusted to 7.4 with NaOH.

Ca^{2+} Indicator Loading and Exposure to AMT. Myocytes were loaded with Fura-2 acetoxymethyl ester (Fura-2 AM; Invitrogen) as described previously (Knollmann et al., 2006). Myocytes were then incubated with AMT (0, 0.5, 1, 3, 10, 300 μM; Sigma) in 5 mM Ca^{2+} Tyrode's solution for 15 min before the experiments and then studied in the presence of AMT for up to 2 h. Thus, on average, myocytes were exposed to the respective AMT concentration for approximately 1 h. Experiments were conducted in a parallel study design with respect to different drug concentrations, which were in turn random in sequence to minimize the effect of time when cells

were studied after isolation. Data from multiple days were pooled for analysis. All experiments were conducted at room temperature (23°C).

Ca^{2+} Fluorescence Measurements. Healthy quiescent Fura-2 loaded rod-shaped isolated ventricular myocytes were loaded in the experimental chamber, and superfused with Tyrode's solution containing 5 mM Ca^{2+} and the desired AMT concentration. Intracellular diastolic Ca^{2+} fluorescence signal and myocyte sarcomere length were simultaneously measured using a dual beam excitation fluorescence photometry set-up (IonOptix, Milton, MA). Before measurement of store Ca^{2+} load, two 10-s recordings of Ca^{2+} fluorescence and cell length were obtained from each myocyte to capture spontaneous SR Ca^{2+} release events. The SR Ca^{2+} content for each myocyte was estimated from the amplitude of the caffeine-induced Ca^{2+} transient during 4-s exposure to Tyrode's solution containing 10 mM caffeine as described previously (Knollmann et al., 2006).

Analysis of Spontaneous SR Ca^{2+} Release Events. The spontaneous SR Ca^{2+} release events (SCRs) were recorded from individual myocytes exposed to increasing AMT concentration. A SCR was defined as any increase in Ca^{2+} fluorescence signal (F_{ratio}) of 0.1

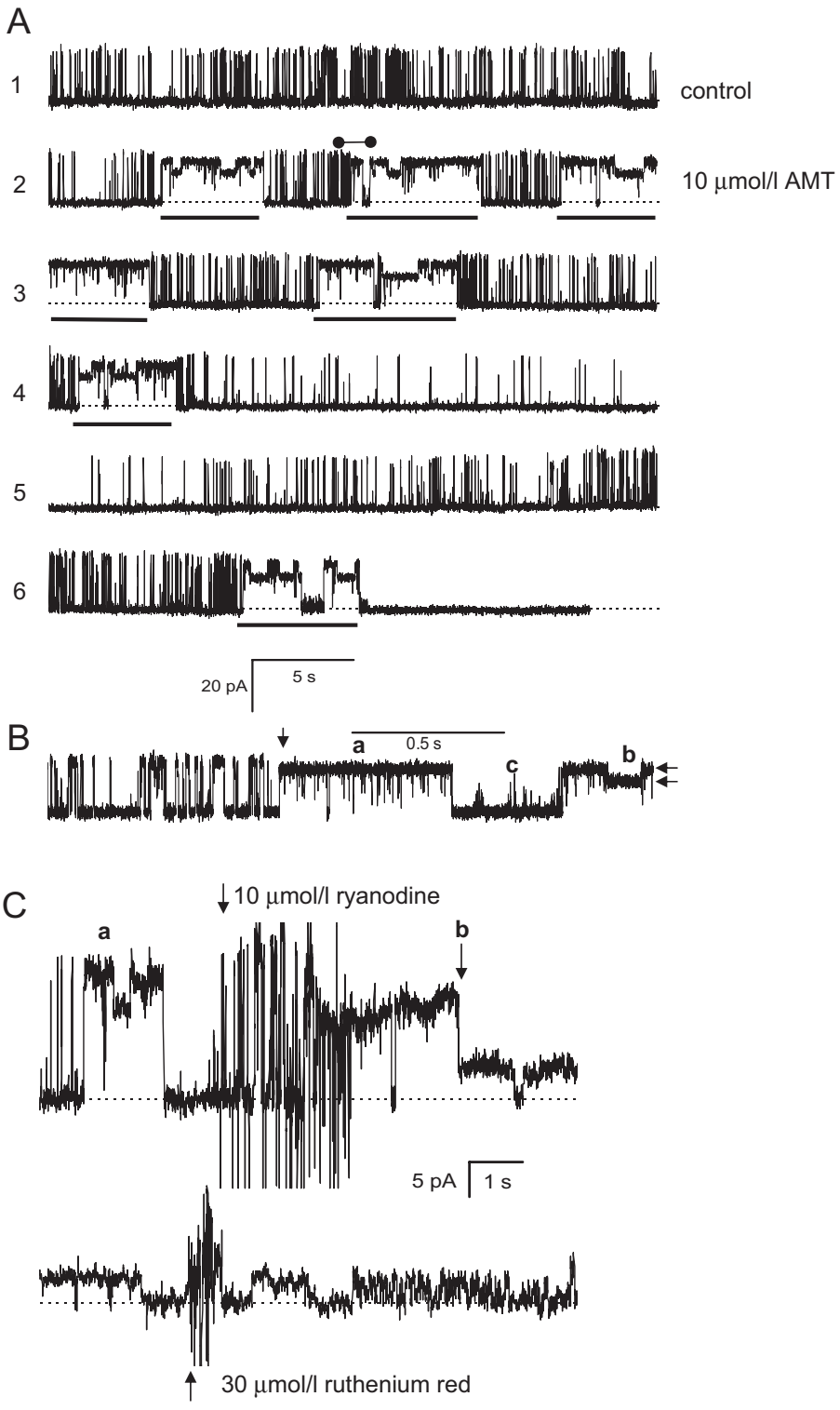

Fig. 1. AMT activates cardiac RyR2s isolated from sheep. A, a single-channel recording of RyR2 from sheep heart representative of 5 experiments obtained at +40 mV (1 kHz filter). Dashed lines indicate the current baseline. The *cis* bath contained 2 mM ATP and 1 μM free Ca^{2+} (2 mM BAPTA + 1 mM $CaCl_2$). The top trace shows channel activity in the absence of AMT. The lower traces show continuous recordings of the same channel after the addition of 10 μM AMT. AMT induces bursts of channel activity (underscored by bars) separated by control-like channel activity. B, a section of recording from the second trace in A (●–●) shown on the expanded time scale (2-kHz filter). The vertical arrow marks the time when the RyR switches between control-like activity and an AMT induced burst. Horizontal arrows mark two prominent subconductance states present in AMT induce burst activity. C, the AMT induced channel responds to cytoplasmic ryanodine and ruthenium red as expected for a RyR. Top trace shows the addition of ryanodine to a channel that exhibits AMT induced bursts (a). Shortly after ryanodine addition (note the stirring noise), the channel enters a substate (b) that is characteristic of ryanodine binding to the RyR. The bottom trace shows the addition of ruthenium red to the same ryanodine modified channel. Ruthenium red causes a flicker block that progresses into total inhibition of the channel after 10 s.

ratiometric units (three times the average background noise) or more from the baseline diastolic signal other than when triggered by caffeine. All SCRs during a 40-s recording period from individual myocytes were counted and reported as an average number of events/s.

In a subset of experiments, SCRs were also recorded from myocytes exposed to 0 and 1 μM AMT in Na^+ and Ca^{2+} free extracellular solutions to prevent any confounding from trans-sarcolemmal Ca^{2+} fluxes. During these experiments, the myocytes were first loaded in 5 mM Ca^{2+} Tyrode's solution to load the SR. The composition of the 0 Ca^{2+}, 0 Na^+ Tyrode's solution was 134 mM LiCl, 5.4 mM KCl, 1 mM $MgCl_2$, 1 mM EGTA, 10 mM glucose, and 10 mM HEPES, pH adjusted to 7.4 with LiOH.

Measurement of SR Ca^{2+} Leak. SR Ca^{2+} leak was measured in myocytes exposed to 0 and 1 μM AMT in 0 Ca^{2+}/0 Na^+ Tyrode's solution to eliminate trans-sarcolemmal Ca^{2+} fluxes (Shannon et al., 2002). After achieving steady state, the external solution was quickly changed to one containing 1 mM tetracaine in Tyrode's solution 0 Ca^{2+}/0 Na^+ for 20 s. Tetracaine blocks the RyR2 causing a drop in cellular Ca^{2+} fluorescence, which represents shift of Ca^{2+} from the cytosol into the SR. The tetracaine-induced drop in diastolic Fura-2 fluorescence ratio was used as an estimate of SR Ca^{2+} leak, as described previously (Shannon et al., 2002).

Measurement of AMT by Electrospray Ionization/LC/MS/MS. To determine optimal instrument parameters for measurement of AMT, 100 μM AMT was infused into a Quantum TSQ triple quadrupole mass spectrometer operating in positive ion mode. Collision induced disassociation of the m/z 278 [M+H$^+$] ion for AMT produced ions of m/z 233 (−18 eV), 202 (−56 eV), 191 (−26 eV), and 91(−38 eV). A similar strategy was employed to determine the optimal product ions for the internal standard imipramine (IMP). Collision induced disassociation of the m/z 281 [M+H+] ion for IMP produced ions of m/z 208 (−30 eV), 193 (−48 eV), 86 (−14eV), and 58 (−56eV).

A standard curve was prepared using 25 μl of 10 μg/ml IMP (0.89 nmol) spiked into 100-μl samples of 0 to 300 μM AMT. Eight hundred and seventy-five microliters of 3% NH_4OH was then added to each sample, and 6 ml of n-hexanes were added to extract AMT and IMP. The hexane (upper) layer was dried down and resuspended in 100 μl of methanol. Samples were analyzed by LC/MS/MS using a C18 column (column volume, ~25 μl; Magic Bullet C18 column 3 μ, 100 Å; Michrom BioResources, Auburn, CA) with the gradient programmed from 60% solvent A (0.5% NH_4OH in water) and 40% Solvent B (0.5% NH_4OH in methanol) to 100% B over 2.5 min and

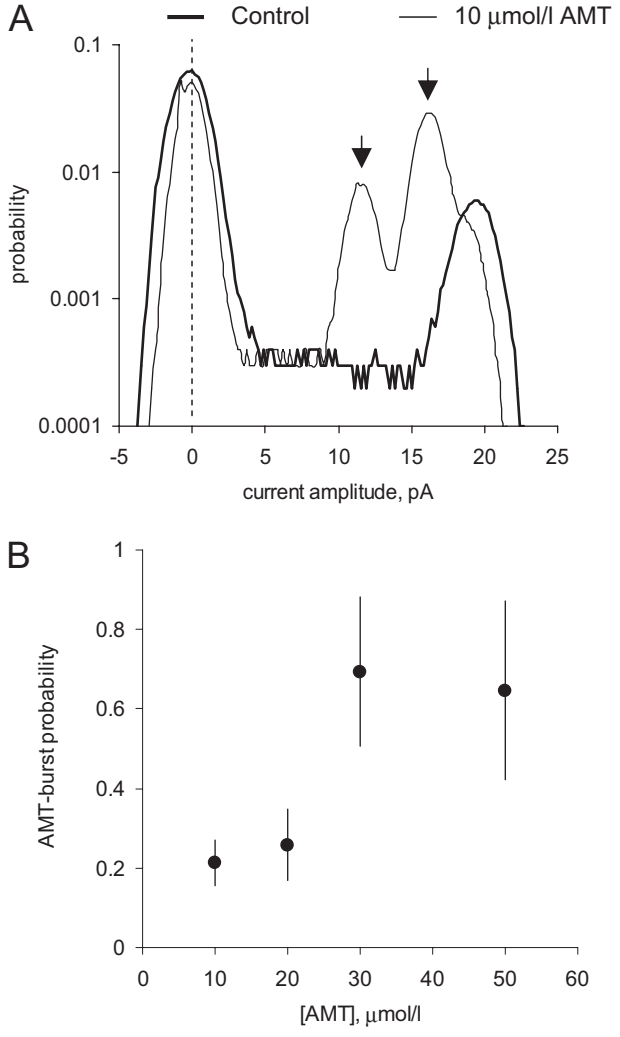

Fig. 2. Properties of AMT-induced bursts under conditions described in Fig. 1. A, current amplitude distributions from single-channel recordings in Fig. 1A. Control recording taken from trace 1 and those in the presence of AMT from traces 2 to 6. AMT induced channel substates are indicated by peaks in the distribution (arrows). B, the dependence of AMT-induced bursts probability on concentration. Burst probability was calculated from the ratio of the total burst duration and the record length.

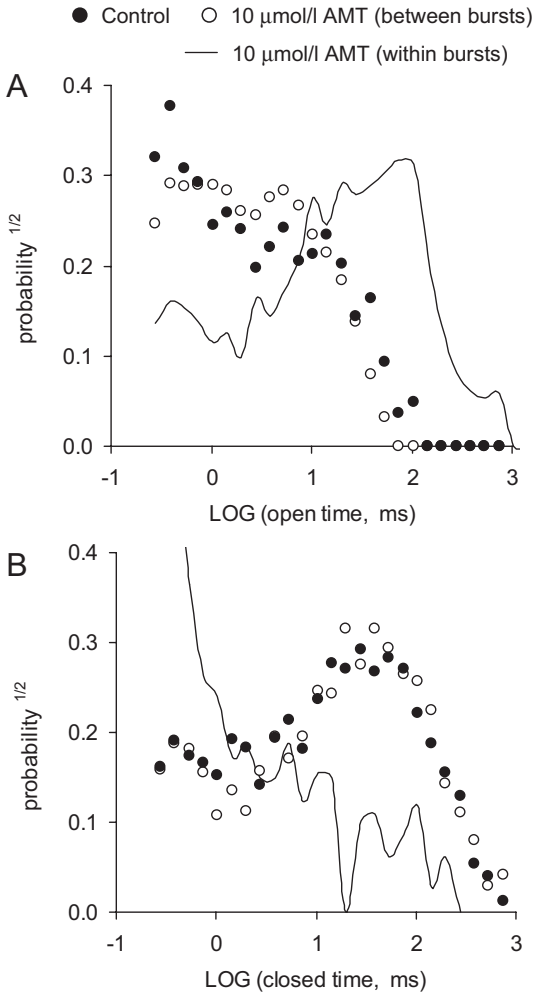

Fig. 3. Open (A) and closed (B) dwell-time histograms from single-channel recordings in Fig. 1A. The data are plotted using the log-bin method (Sigworth and Sine, 1987) using log-bins with seven per decade (2 kHz filter). ●, dwell-times from control activity in the top trace of Fig. 1A. ○, dwell-times from control-like activity between AMT induced bursts in the second and third traces in Fig. 1A. Curves, dwell-times from all the AMT-induced bursts shown in Fig. 1A.

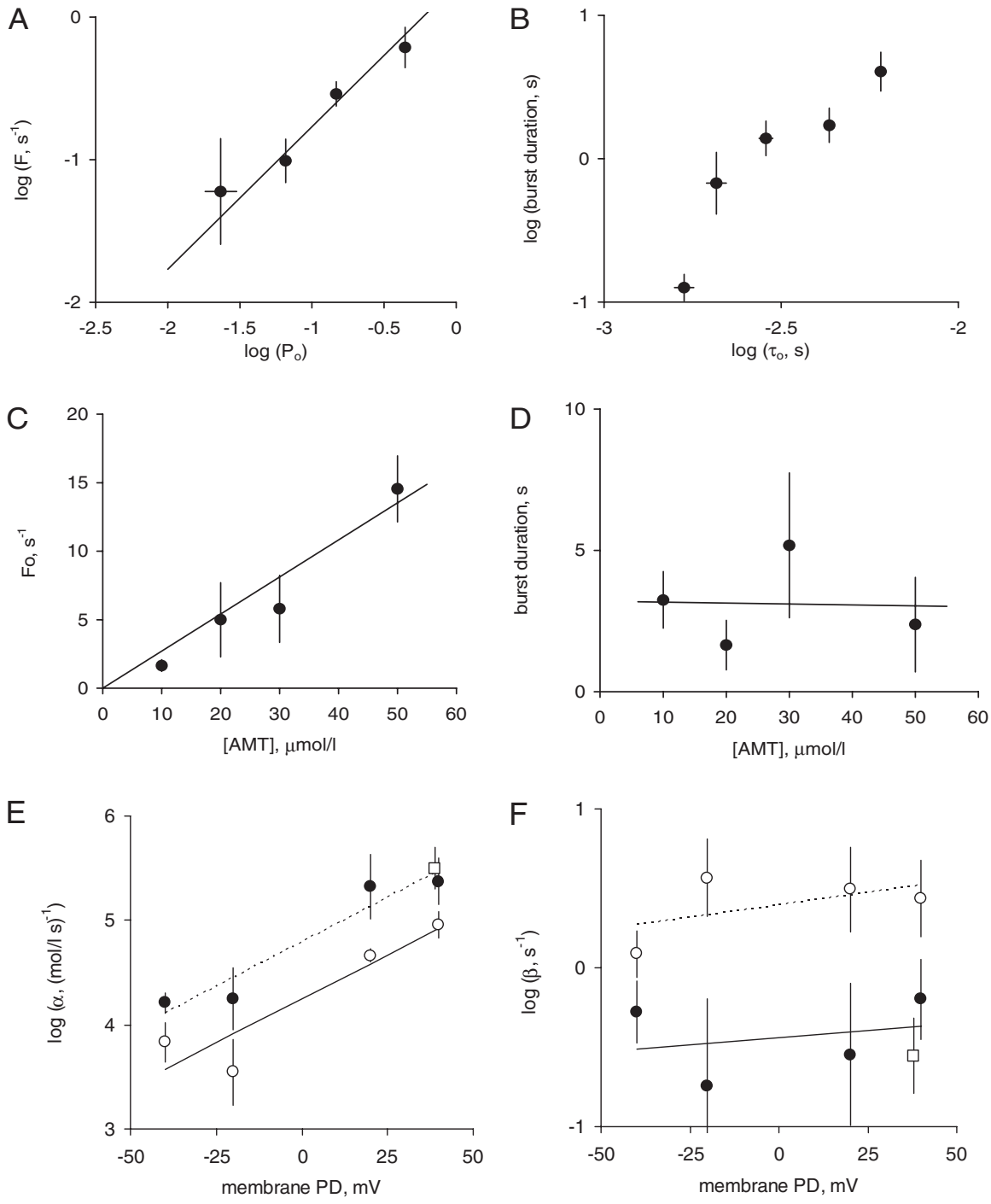

Fig. 4. The properties of AMT induced openings (bursts) in cardiac RyR2s from sheep and mouse heart. The effects on sheep RyR2 of AMT in the *cis* (●) or *trans* (○) baths and *cis* AMT on mouse RyRs [$Casq^2$(+/+), □] were measured in the presence of 2 mM ATP and 1 μM free Ca^{2+} (2 mM BAPTA + 1 mM $CaCl_2$) and at +40 mV (unless specified otherwise). A, the correlation between burst frequency (F = reciprocal of the interburst interval) on the open probability of the channel during the burst interval in the presence of 10 μM AMT. The data are grouped (n = 4–18) from 50 inter burst intervals from 6 sheep RyR2s and from 12 inter burst intervals from two mouse RyR2s. (Channels under control conditions normally exhibit fluctuations in P_o, τ_o, and τ_c under steady experimental conditions, see text for details). The line depicts the least-squares fit of the equation $F = P_o k_+$ to ● with $k_+ = 1.7 \pm 0.4\ s^{-1}$ (the intercept at $P_o = 1$). B, the correlation between burst duration and τ_o during the preceding burst interval derived from the same single channel data as used for A. C and D, derivation of rate constants for AMT association, α, and dissociation, β, from the concentration-dependencies of F_o (the reciprocal of the total open period between bursts) (C) and burst duration (D). The data points show the mean and S.E.M. of three to six measurements. C-line, the fit of $\alpha = F_o$/[AMT] to the data where the slope = $\alpha = 0.27 \pm 0.025\ \mu M \cdot s^{-1}$ and the intercept = 0. (D line) Linear fit to the data with slope = $-0.003 \pm 0.06\ \mu M \cdot s^{-1}$, intercept = $\beta^{-1} = 3.2 \pm 2.0$ s. E and F, voltage-dependencies of α and β from luminal (*trans*) and cytoplasmic (*cis*) sides of the membrane. In E and F, the data points show the mean and SEM of three to eight measurements and linear fits to the sheep log-data are shown as solid lines. Line parameters are: E (solid) slope = $0.017 \pm 0.003\ mV^{-1}$, intercept = -4.2 ± 0.1; E (dashed) slope = $0.017 \pm 0.005\ mV^{-1}$, intercept = -4.75 ± 0.16; F (solid) slope = $0.002 \pm 0.004\ mV^{-1}$, intercept = -4.4 ± 0.2; F (dashed) slope = $0.003 \pm 0.003\ mV^{-1}$, intercept = -0.4 ± 0.1.

then continuing at 100% B. Flow rate was 200 μl/min. Eluent was coupled directly to the mass spectrometer operated in selective reaction monitoring positive ion mode monitoring the selective reaction monitoring transition m/z 278 → 191 at −26 eV for AMT and m/z 281 → 193 at −48 eV for IMP. Both compounds eluted at approximately 2.4 min. The standard curve gave a linear response ($R^2 = 1.0$) with moles of AMT = $8 \times 10^{-10} \times$ (ratio area of m/z 278 ion peak/area of m/z 281 ion peak) − 1.5×10^{-11}.

Measurement of Intracellular AMT Concentration. Isolated myocytes were incubated with 0 to 300 μM AMT in 5 mM Ca^{2+} Tyrode's solution for 1 h. Because all the isolated myocytes experiments were done within 2 h of AMT exposure, it was considered apt to measure intracellular AMT concentration at the mean time of 1 h. Each concentration was performed in triplicate. After this incubation period, the cells were washed three times in 5 mM Ca^{2+} Tyrode's solution to remove extracellular AMT. The pelleted myocytes were weighed and then resuspended in 1 ml of 3% NH_4OH. Twenty-five microliters of 10 μg/ml IMP was added as an internal standard, and then 6 ml of *n*-hexanes were added to extract the AMT and IMP. The hexane (upper) layer was dried down and resuspended in 100 μl of methanol. AMT was quantified by LC/MS/MS as described above. The intracellular concentration of AMT was calculated as moles of AMT in the sample determined by LC/MS/MS divided by the pelleted cell volume of the sample using a density of 1 μl per 1 mg of pellet weight.

Statistical Analysis. Experiments on SR Ca^{2+} release were done in random sequence with respect to AMT concentrations. Differences between groups were assessed using a one-way analysis of variance. If statistically significant differences were found, individual groups were compared with Student's *t* test or by nonparametric tests as indicated in the text. Results were considered statistically significant if the *P* value was less than 0.05. Unless otherwise indicated, results are expressed as arithmetic means and S.E.M.

Results

AMT Directly Activates RyR2 Channels in Lipid Bilayers. First, we determined the effect of increasing cytoplasmic (i.e., cis) AMT concentration on native RyR2 channels isolated from sheep heart in the presence of *cis* 2 mM ATP and 1 μM Ca^{2+} (systolic [Ca^{2+}]) at a holding potential of 40 mV (Fig. 1). Channels were responsive to ryanodine and ruthenium red, which identifies them as RyRs (Fig. 1C). In the absence of AMT, sheep RyR2 had a P_o of 0.31 ± 0.09, mean open time (τ_o) of 6.7 ± 1.0 ms, and mean closed time (τ_c) of 14 ± 7 ms, and peak current (*I*) of 18.4 ± 0.8 pA ($n = 5$) (e.g., Fig. 1A, top trace). Addition of AMT (10 μM) caused intermittent bursts of extended channel openings (Fig. 1A, underscored sections in traces 2–6) amid channel activity that was indistinguishable from control. Analysis of sections of channel activity between bursts in traces 2 and 3 gave $P_o = 0.14 \pm 0.04$, $\tau_o = 4.0 \pm 0.4$ ms, $\tau_c = 25 \pm 8$ ms, and $I = 18.2 \pm 0.7$ pA ($n = 5$). The AMT induced bursts exhibited markedly different conductance and gating properties to control activity (Fig. 1B, features a–c). Amplitude histograms of channel events show that these bursts had two prominent conductance levels (Fig. 2A, arrows) corresponding to 60 and 85% of the maximal conductance RyR2 in the absence of AMT. The 85% conductance level exhibited very brief channel closures (<1 ms; Fig. 1Ba), whereas during the 60% level, channel closures were rare (Fig. 1Bb). The channels also had periods of channel closures with brief openings (Fig. 1Bc). The probability of these AMT-induced bursts increased from 0.2 to 0.8 over the concentration range 10–50 μM (Fig. 2B).

Figure 3 shows dwell-time histograms of channel openings (Fig. 3A) and closures (Fig. 3B) in the absence and presence of AMT. (All histograms could be fitted by the sum of two exponentials, fits not shown.) The AMT induced bursts has

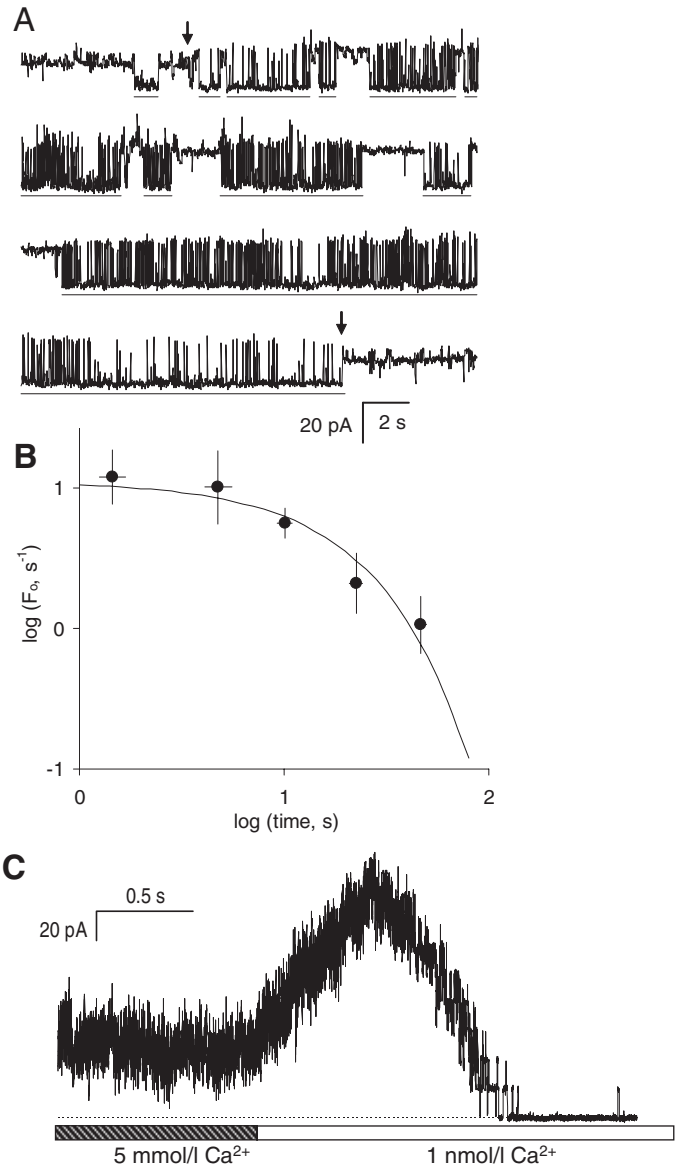

Fig. 5. Slow reversal of AMT activation upon washout. A, a continuous recording of RyR2 activity in the presence of cytoplasmic 1 μM Ca^{2+} and 2 mM ATP obtained at +40 mV. At the beginning of the recording, RyR2s were exposed to 50 μM AMT that had been added to the cytoplasmic bath. Under these conditions, AMT nearly fully activated the RyR2. Interburst periods are indicated by horizontal bars. The first arrow indicates when AMT was washed away by flowing AMT-free solution onto the bilayer. AMT-induced bursts continued to occur after perfusion albeit at a reduced frequency. The second arrow indicates when perfusion was turned off and AMT regained access to the RyR2. B, summary of burst frequency with respect to RyR2 opening, F_o, at different time points after perfusion was initiated. Data were obtained from a total of 9 perfusion cycles on four RyR2s. The solid curve shows an exponential fit with a decay constant of 17 ± 4 s and with $F_o = 11 \pm 4$ s^{-1} at time 0. C, a control experiment demonstrating that solution exchange occurs in ~1 s. Ten RyRs in the bilayer were initially exposed to 5 mM Ca^{2+} in the cytoplasm (RyRs were partially inhibited by a low-affinity Ca^{2+} inhibition). Perfusion was used to exchange the bath for one that contained <1 nM Ca^{2+} (5 mM BAPTA, [Ca^{2+}] is too low to activate RyRs). On initiating solution exchange, the RyR activity increased as the [Ca^{2+}] reduced to levels for maximal RyR activity (~100 μM) and then RyRs deactivated once [Ca^{2+}] fell below 100 nM.

very different open and closed dwell-time distributions. The mean channel open time in AMT induced bursts was 37 ms, which is 10-fold longer than during control activity (3.4 ms). Mean closed times during bursts were ~30× shorter than control (1.3 versus 35 ms, respectively). The dwell-time histograms obtained from channel activity in between the AMT induced bursts were indistinguishable from those obtained in the absence of AMT (see ○ and ● in Fig. 3). This is consistent with AMT-induced bursts being associated with times when AMT is bound to the RyR and with the notion that during the interburst periods, AMT is not bound.

Kinetics of AMT Activation in RyR2 Channels. We inferred the kinetics of AMT binding by measuring the duration of the AMT induced opening bursts and the intervals between them in RyR2 channels. In the absence of AMT, RyR2 exhibited a well characterized modal gating phenomenon (Zahradníková et al., 1999) in which channels would randomly fluctuate between periods of high and low P_o over periods of tens of seconds. An example of this can be seen in Fig. 1A, where P_o between AMT bursts transiently decreases during trace 3. We also noticed that the separation between AMT induced bursts was generally longer during periods of low RyR2 P_o, suggesting that AMT binding requires that RyRs be open. To quantify this effect we measured the P_o of RyRs during each interburst period. We then correlated the reciprocal of each burst gap duration (i.e., burst frequency, F) with the P_o of the RyR2 during that gap (Fig. 4A). This analysis shows that F and P_o are proportional over a wide range of P_o. In other words, long burst gaps are associated with low P_o. The linear correlation between F and P_o confirms that AMT induced bursts are primarily initiated during the open channel configuration. We derived the association rate of AMT, k_+, by fitting the correlation between F and P_o with the equation $F = P_o\, k_+$ (see line and ● in Fig. 4A). This equation can be recast into the form $F_o = k_+$, where F_o is the reciprocal of the mean total open time between bursts. We also calculated the dissociation rate, k_-, which is equal to the reciprocal of mean burst duration provided that the duration of AMT induced bursts reflects the period that AMT is bound to the RyR. We note that the duration of AMT-induced bursts were shorter after interburst periods of RyR2 activity with relatively low mean open time (τ_o; Fig. 4B) indicating a link between RyR2 closing rate in the absence of AMT and k_-.

Increasing AMT concentration up to 50 μM caused a proportional increase in F_o but had no significant effect on the burst durations (Fig. 4, C and D). Once again, this is consistent with an AMT activation mechanism in which the bursts represent periods during which AMT is bound to the RyR2 and that AMT binding occurs mainly while the channel is open. The association rate constant, α, is calculated from the [AMT] dependence of F_o using the equation $\alpha = F_o/[\text{AMT}]$ ($F_o = k_+$). The dissociation rate constant, β, was equal to k_-. Linear fits to the data in Fig. 4, C and D gives values for the rate constants of $\alpha = 0.27 \pm 0.025\ (\mu\text{M} \cdot \text{s})^{-1}$ and $\beta = 0.3 \pm 0.2\ \text{s}^{-1}$ (+40 mV). We found that α was strongly voltage-dependent, whereas β showed no significant dependence on voltage (Fig. 4, E and F, ●). We also measured the frequency and duration of AMT induced bursts in mouse wild-type (*Casq2*(+/+)) RyR2 under the same conditions as we did for sheep RyRs and found that AMT binding kinetics were not significantly different between RyRs from mouse and sheep (see □ and ● in Fig. 4, E and F).

We investigated the possibility of a luminal facing AMT site on the RyR2 by applying AMT to the luminal (*trans*) bath. We found that AMT induced bursts of channel openings with conductance levels identical to those induced by cytoplasmic AMT (records not shown). Moreover, the slopes of the voltage-dependencies of the rates for AMT association and dissociation were not significantly different for luminal and cytoplasmic AMT. The only difference was that, at a given voltage, the RyR2 was slightly less sensitive to luminal AMT (i.e., AMT had a lower association rate and higher dissociation rate from the luminal side, Fig. 4, E and F, ○).

Because luminal and cytoplasmic AMT had nearly identical effects on RyR2 activity, it is likely that the same AMT binding site is accessible from both sides of the membrane. AMT partitions into the bilayer such that the hydrophobic portion of the molecules incorporates into the acyl chains of the lipids and the charged amino group resides among the polar heads groups (Deo et al., 2004). This study showed that the mole fraction of AMT in the bilayer is ~0.01 when its concentration in the bath was 10 μM. Therefore we considered the possibility that AMT can adsorb to bilayers and/or permeate them before reaching its site of action. To test for this, we measured the rate of reversal of the AMT effect after washout of the drug from the cytoplasmic bath. Compounds can be washed out of the bath within ~1 s as we show in Fig. 5C. However, drugs that partition into the bilayer are slow to exchange with the aqueous phase and could be retained in the lipids for some time after they have been removed from the bath. Reversal of AMT activation of RyR2s was assessed by measuring RyR2 burst frequency (F_o) at different time points after perfusion was initiated (Fig. 5A). RyR2s were initially exposed to 50 μM AMT via aliquot addition to the cytoplasmic bath. When the bilayer and RyR2 were perfused with AMT-free solution so that AMT had been removed from the vicinity of the bilayer (see *Materials and Methods*) AMT-induced bursts continued to occur for several minutes. Figure 5B shows accumulated data obtained from several RyR2s exposed to two to six repeats of 2-min episodes of bath perfusion. Repeats were achieved by switching off the perfusion to allow AMT to gain access to the bilayer and RyR2. During perfusion, F_o declined exponentially with a decay constant of 17 ± 4 s (equivalent to a 12-s half-time). This is considerably

TABLE 1

The effects of cytoplasmic [Ca^{2+}] and [Mg^{2+}] on the properties of AMT-induced openings (bursts) in RyR2s from sheep heart

The cytoplasmic bath contained 2 mM ATP plus the indicated free concentrations of Ca^{2+} and Mg^{2+}. Frequency of bursts was derived from either the reciprocals of total time between bursts (F) or the total open time between bursts (F_o). F and F_o are proportional to [AMT] and the proportionality constants are listed. P_o and τ_o are the open probability and mean open time of the channel activity between bursts, respectively. n = number of separate recordings from which data were obtained.

Cytoplasmic Conditions	F/[AMT]	F_o/[AMT]	Burst Duration	P_o	τ_o	n
	$\mu M^{-1} \cdot s^{-1}$	$\mu M^{-1} \cdot s^{-1}$		s	ms	
1 μM Ca^{2+}	0.012 ± 0.003	0.27 ± 0.03	4.2 ± 1.4	0.044 ± 0.018	3.7 ± 1.4	6
0.1 μM Ca^{2+}	0.0016 ± 0.0002	0.18 ± 0.06	7.8 ± 1.7	0.008 ± 0.003	3.9 ± 1.2	3
0.1 μM Ca^{2+}, 220 μM Mg^{2+}	0.0004 ± 0.0002	0.32 ± 0.15	2.2 ± 1.4	0.0013 ± 0.0004	2.1 ± 0.7	3

slower than the time course of AMT washout from the aqueous phase (<1 s half-time), which indicates either that 1) AMT binds to the RyR2 from within the bilayer or 2) the membrane lipids provide a reservoir of AMT to activate RyR2s. We argue for the latter possibility (see *Discussion*)

Because the binding of AMT depends on the open conformation of the RyR2, we examined the effect on AMT binding of cytoplasmic Ca^{2+} and Mg^{2+}, which are known to modulate the P_o of RyR2. The effects of Ca^{2+} and Mg^{2+} on the duration and frequency of AMT induced bursts are summarized in Table 1. Reducing [Ca^{2+}] from 1 to 0.1 μM caused a 7-fold decrease in the AMT bursting rate [$F/(\mu M)$], whereas the association rate to the open state [$F_o/(\mu M)$] was not significantly affected. These results are in line with the effect of P_o on AMT binding shown in Fig. 4A. Moreover, decreasing [Ca^{2+}] decreased burst duration in association with a decrease in τ_o similar to that seen in Fig. 4B. A similar pattern occurred with Mg^{2+}, where the addition of Mg^{2+} (220 μM free Mg^{2+} in the presence of 0.1 μM Ca^{2+}) to the cytoplasmic bath decreased RyR2 P_o and τ_o in conjunction with a decreased AMT bursting rate and duration. Once again, F_o was not significantly affected by Mg^{2+}. Thus it seems that AMT is more able to bind to and modify RyR2 gating under conditions in which the RyR2 are more active.

AMT Activates RyR2 at Low Concentrations and Inhibits Them at High Concentrations. RyR2 activation and inhibition (sheep RyR2) was also seen in single-channel recordings in the presence of 1 μM Ca^{2+} (Fig. 6, A and B). At concentrations up to 200 μM, AMT induced long-lived substates in the channel record just as shown in Figs. 1 and 5. However, at higher concentrations (500 and 1000 μM), AMT caused brief channel closures that gave the recordings a flickery appearance. The inhibitory effect of AMT was similar at both +40 mV and −40 mV, indicating that inhibition is not voltage-dependent like the AMT activation process. These data demonstrate that AMT has a high-affinity activation site and a lower affinity inhibition site. The inhibitory action of AMT at such high concentrations was not studied in detail because it is unlikely to be important to the clinical action of this drug.

AMT Does Not Require the Presence of Casq2 to Activate RyR2 Channels. Because AMT is known to bind to Casq2 (Park et al., 2005), and Casq2 prominently regulates RyR2 channel open probability (Gyorke et al., 2002), we investigated the possibility that Casq2 is the binding site responsible for the AMT induced channel opening we observe. Thus, we determined the effect of increasing cytoplasmic (i.e., cis) AMT concentration on RyR2 channels isolated from *Casq2*(+/+) and *Casq2*(−/−) mice in the presence of *cis* 2 mM ATP and 0.1 μM Ca^{2+} (diastolic [Ca^{2+}]) at a holding potential of 40 mV (Fig. 7A and B). RyR2 from *Casq*^{2}(+/+) mouse heart had a P_o of 0.042 ± 0.018, mean τ_o of 1.9 ± 0.5 ms, and mean τ_c of 210 ± 120 ms (n = 6). In the *Casq2*(−/−) RyR2, the mean P_o was 0.0180 ± 0.0086, mean τ_o of 3.5 ± 1.5 ms, and mean τ_c of 633 ± 320 ms (n = 7). Even though generally lower, the P_o of RyR2 from *Casq2*(−/−) hearts was not significantly different from those derived from *Casq2*(+/+) mouse (p = 0.11). The RyR2 maximum current was also not significantly different between *Casq2*(+/+) (16.1 ± 0.4 pA at +40 mV) and *Casq2*(−/−) mice (16.2 ± 0.5 pA at +40 mV).

AMT concentrations of 5 to 10 μM produced its typical bursting phenomenon in RyR2 channels, regardless of whether Casq2 was present or not (Fig. 7, A and B). AMT-induced bursts had extended openings with two prominent conductance levels corresponding to 70 and 90% of the maximal conductance RyR2 in the absence of AMT. In RyR2 from both *Casq*^{2}(+/+) and *Casq2*(−/−) mice, AMT increased P_o by 4- to 6-fold at 5 to 10 μM (Fig. 7C). This activation was mediated mainly by an increase in τ_o. Thus, AMT binding to Casq2 is not necessary for AMT activation of RyR2 channels.

AMT Reduces SR Ca^{2+} Content in Intact Myocytes. To assess the consequences of AMT's effects on RyR2 channels in intact myocytes, we loaded isolated mouse ventricular myocytes with the Ca^{2+} fluorescent indicator Fura-2 AM and exposed the myocytes to increasing concentrations of AMT.

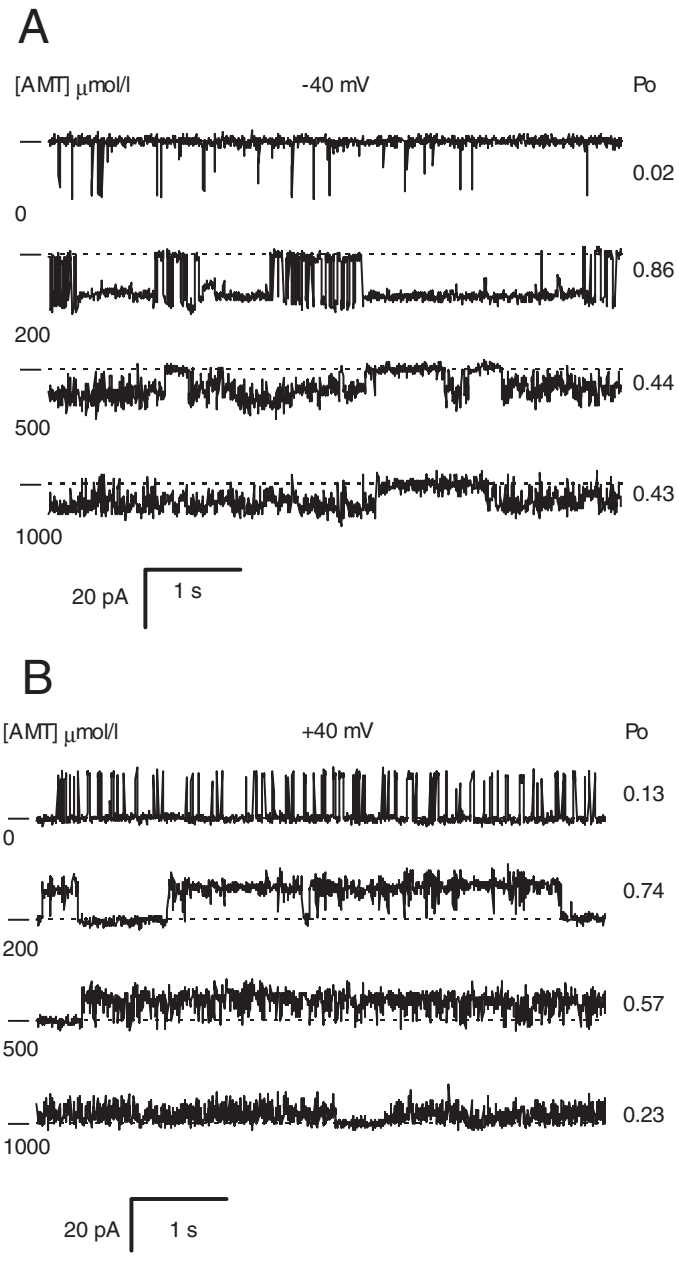

Fig. 6. Single-channel recordings of RyR2s from sheep heart representative of four experiments obtained at −40 mV (A) and +40 mV (B). The dashes at the left of each record indicate the current baseline. The AMT concentrations in the *cis* bath are listed at the left of each trace and the open probability of the channels at the right. The *cis* bath also contained 2 mM ATP and 1 μM free Ca^{2+} (2 mM BAPTA + 1 mM $CaCl_2$).

High extracellular Ca^{2+} (5 mM) was used to maximally load the SR with Ca^{2+} and thereby enhance our ability to detect any effects of AMT on SR Ca^{2+} handling. SR Ca^{2+} content was estimated by rapid exposure to caffeine (10 mM) and the amplitude of the caffeine-induced Ca^{2+} transient was taken as a measure of SR Ca^{2+} content (Fig. 8A). AMT reduced SR Ca^{2+} content in a concentration-dependent manner, suggesting that its activation of RyR2 channels depletes SR Ca^{2+} stores (Fig. 8, A and B).

AMT Causes Spontaneous SR Ca^{2+} Release. To further probe the mechanism of reduction in SR Ca^{2+} content induced by AMT, we analyzed SCRs in intact mouse ventricular myocytes exposed to increasing AMT concentrations (Fig. 9A). We have shown previously that SCRs are caused by increased Ca^{2+} leak from the SR and are associated with ventricular arrhythmias (Knollmann et al., 2006; Chopra et al., 2007).

The rates of SCRs increased significantly from control condition (0 μM AMT) to 0.5 and 1 μM AMT in a concentration-dependent fashion, with a 4-fold increase observed at 1 μM AMT in myocytes (Fig. 9B). The increase in SCRs probably contributes to reduction of SR Ca^{2+} content at concentrations <3 μM (Fig. 8B). However, at high concentrations of AMT (>3 μM), the rate of SCRs started to decline (Fig. 9B), probably due to concentration-dependent decline in SR Ca^{2+} content (Fig. 8B). Consistent with the SR calcium depletion and increased rate of SCRs, AMT at 1, 3, and 10 μM also significantly increased diastolic Ca^{2+} (average diastolic Fura2 fluorescence ratio at respective AMT concentration: 0 μM, 1.07 $\pm$ 0.02; 1 μM, 1.22 $\pm$ 0.03; 3 μM, 1.14 $\pm$ 0.03; 10 μM, 1.25 $\pm$ 0.03; $p < 0.01$ compared with 0 μM). AMT concentrations >10 μM had no significant effect on diastolic Ca^{2+}, probably as the result of their profound SR Ca^{2+} depletion during the incubation period.

To probe the relationship of SCRs and SR Ca^{2+} content upon exposure to AMT, we next examined the effect of 1 μM AMT in myocytes with different SR Ca^{2+} content. As expected from the regulation of RyR2 by SR luminal Ca^{2+} (Gyorke et al., 2002), the rate of SCRs increased with increasing SR Ca^{2+} load. AMT significantly increased the rate of SCRs at all SR Ca^{2+} contents examined (Fig. 9C).

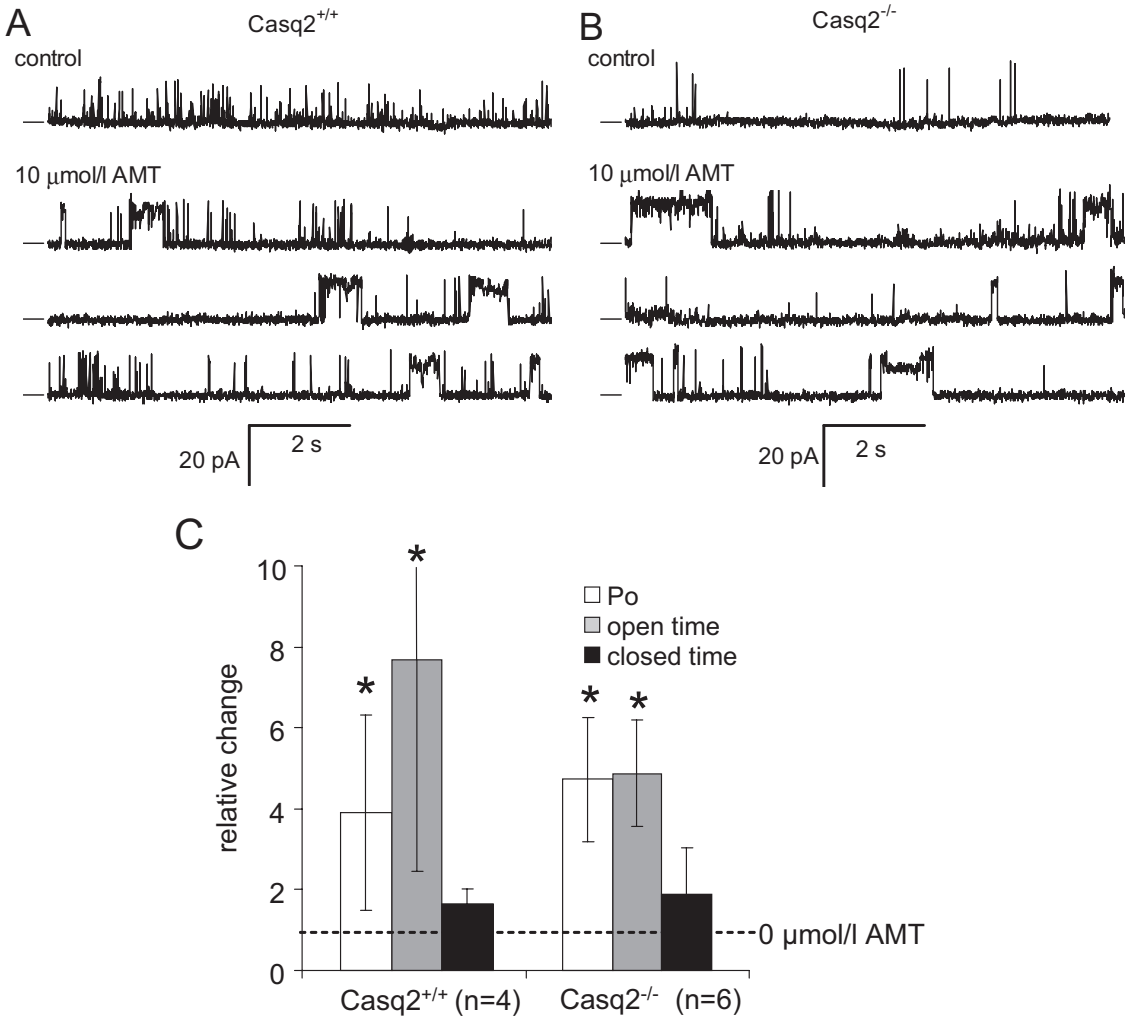

Fig. 7. AMT activates cardiac RyR2s isolated from *Casq2*(+/+) and *Casq2*(−/−) mice. The effects of AMT in the *cis* (cytoplasmic) bath were in the presence of 2 mM ATP and 0.1 μM free Ca^{2+} (4.5 mM BAPTA + 1 mM $CaCl_2$). The *trans* (luminal) bath contained 0.1 mM Ca^{2+}. A and B, single-channel recordings of RyR2s at +40 mV. The top traces show channel activity in the absence of AMT (control). The bottom three traces are continuous recordings obtained in the presence of 10 μM AMT. The dashes at the left of each record indicate the current baseline and channel openings are upward transitions from the baseline. Amitriptyline induced long-lasting openings of at least two conductance levels. C, pooled results showing the relative effect (normalized to control levels) of 5 to 10 μM AMT on RyR2 P_o, mean τ_o, and mean τ_c. The number of samples in the means is given in parentheses.

Rapid depletion of SR Ca^{2+} content with caffeine (10 mM) abolished SCRs until the SR refilled (data not shown), suggesting the SR as the source of SCRs. Furthermore, the SCRs were reminiscent of a low-dose (500 μM) caffeine effect on RyR2 channels (Venetucci et al., 2007). Nevertheless, to exclude any possible contribution of *trans*-sarcolemmal Ca^{2+} influx triggering SCRs, we next quantified SCRs rates in myocytes bathed in Na^+ and Ca^{2+} free extracellular solutions. The rate of SCRs remained significantly higher in the myocytes exposed to 1 μM AMT (Fig. 10, A and B), which demonstrates that the SCRs were the result of intracellular SR Ca^{2+} release and not caused by Ca^{2+} influx across the sarcolemma. Because the Na-Ca exchanger is blocked under these experimental conditions, the amplitude of SCRs was higher compared with experiments in Na^+ containing bath solutions (compare Figs. 9A and 10A). Taken together, these data suggest that AMT activation of RyR2 channels causes the increased rate of SCRs in intact myocytes. Ca^{2+} or Na^+ influx into the myocyte is not required for the effect of AMT.

AMT Increases SR Ca^{2+} Leak in Intact Myocytes. Another predicted consequence of increasing RyR2 channel open probability in intact myocytes is an increase in SR Ca^{2+} leak, which has been associated with SCRs and triggered arrhythmias (Knollmann et al., 2006). Therefore, we next estimated SR Ca^{2+} leak in isolated ventricular myocytes exposed to 1 and 0 μM AMT using the RyR2 channel inhibitor tetracaine (Shannon et al., 2002). Consistent with our hypothesis, we found a significantly increased SR Ca^{2+} leak in myocytes exposed to 1 μM compared with 0 μM AMT (Fig. 10A and C). Thus, AMT concentrations of 1 μM are sufficient to activate RyR2 channels and cause spontaneous SR Ca^{2+} release in intact myocytes.

AMT Accumulates in Myocytes. Compared with its effects on single channels in lipid bilayer, AMT caused an effect in intact myocytes at lower concentrations (0.5 μM versus 5

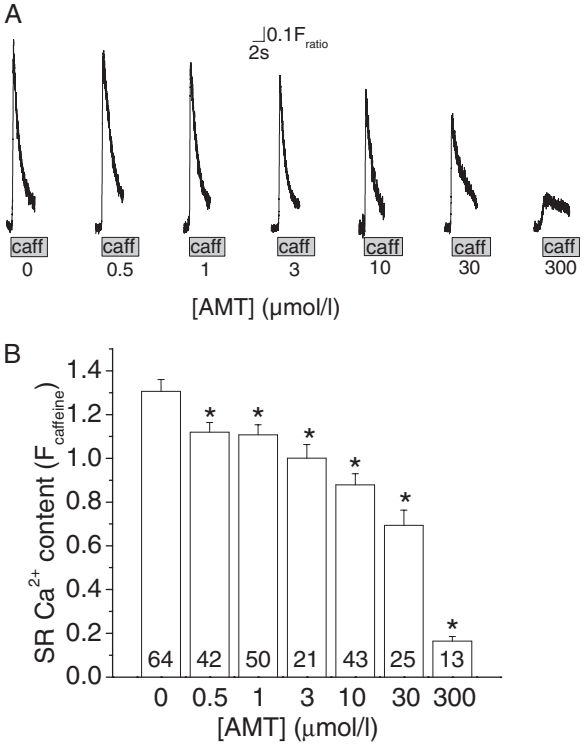

Fig. 8. AMT exposure causes a concentration-dependent reduction in SR Ca^{2+} content in intact myocytes. A, representative examples of rapid caffeine application (10 mM) to Fura-2 loaded myocytes exposed to increasing concentrations of AMT. Myocytes were incubated with respective concentration of AMT for at least 10 min before experiments. The height of the caffeine-induced Ca^{2+} transient was used as a measure of SR Ca^{2+} content. B, average values of SR Ca^{2+} content in myocytes exposed to increasing AMT concentrations (0, 0.5, 1, 3, 10, 30, and 300 μM). Note the concentration-dependent decrease in SR Ca^{2+} content in myocytes. Numbers indicate the number of myocytes examined for each drug concentration. *, $p < 0.05$ for comparison with 0 μM AMT using Student's t test.

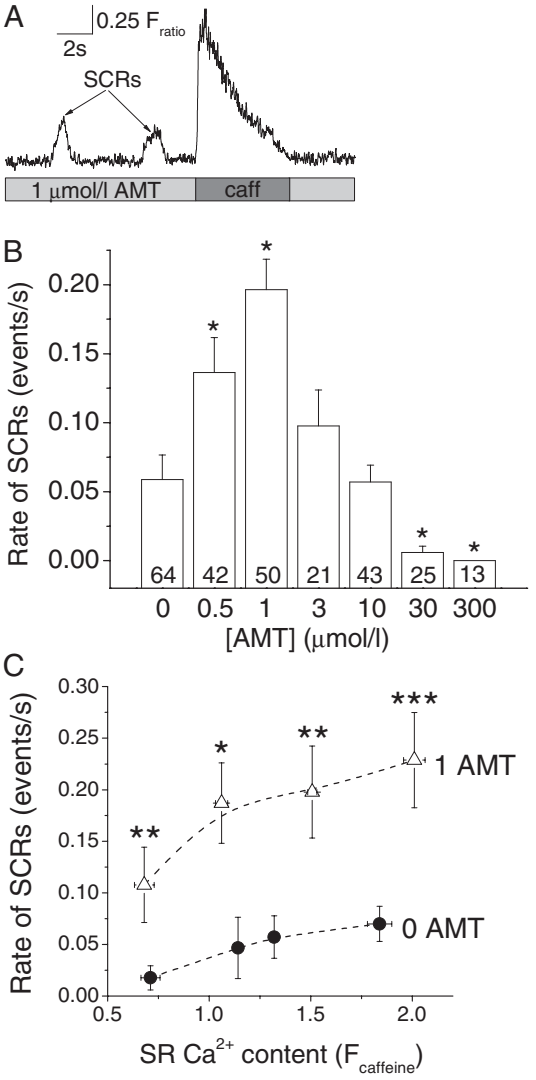

Fig. 9. SCRs in myocytes exposed to increasing AMT concentrations. A, representative examples of SCRs in a Fura-2 loaded myocytes exposed to 1 μM AMT. Upon emptying the SR (rapid exposure to 10 mM caffeine), the SCRs were abolished only to reappear once the SR refilled (data not shown). B, comparison of the incidence of SCRs in myocytes exposed to increasing AMT concentrations. Data represent the average number of SCRs/s during the recording period of 40 s. Note the significant increase in SCRs at 0.5 and 1 μM AMT compared with 0 μM AMT. In contrast, at higher AMT concentrations (>3 μM), there was a decrease in SCRs, probably as a result of decrease in SR Ca^{2+} content (see Fig. 8B). Numbers indicate the number of myocytes examined for each drug concentration. *$p < 0.05$ for comparison with 0 μM using Student's t test. C, dependence of SCR rates on SR Ca^{2+} content in myocytes exposed to 0 and 1 μM AMT. SR Ca^{2+} content was altered by incubating myocytes in solutions with extracellular Ca^{2+} concentrations ranging from 2 to 5 mM. As expected, SCR rates increased with increased SR Ca^{2+} content. Note that 1 μM AMT significantly increased rates of SCR across a wide range of SR Ca^{2+} loads. 0 μM AMT, $n = 99$; 1 μM AMT, $n = 82$; *, $p < 0.05$; **, $p < 0.01$; ***, $p < 0.001$ using Student's t test.

μM, compare Figs. 7 and 8). We next determined the intracellular concentration of AMT in the myocytes by mass spectrometry after 1-h exposure to extracellular AMT. Intracellular AMT concentrations were approximately 5-fold higher than extracellular concentrations at all (0.5–300 μM) AMT concentrations examined (Fig. 11). Thus, intracellular AMT accumulation may contribute to the higher potency of AMT in intact myocytes.

Mg^{2+} Restores SR Ca^{2+} Content and Decreases Rates of SCRs in AMT-Exposed Myocytes. Our bilayer data show that AMT binds preferentially to open RyR2 channels and that reducing RyR2 channel P_o by increasing cytoplasmic Mg^{2+} concentration decreases AMT activation of RyR2 channels (Table 1). Thus, we next tested whether Mg^{2+} can also attenuate AMT-induced effects on SR Ca^{2+} handling in intact myocytes. Myocytes were incubated for 60 min in solutions containing either 1 or 5 mM Mg^{2+} and then exposed to different AMT concentrations. Pretreatment with high Mg^{2+} increased SR Ca^{2+} content in myocytes regardless of whether AMT was present (Fig. 12A), consistent with the stabilizing effect of Mg^{2+} on the RyR2 complex (Laver et al., 1997). It is noteworthy that high Mg^{2+} specifically prevented the AMT-induced increase in SCRs in myocytes (Fig. 12B). Thus, use of Mg^{2+} could be a therapeutic approach in AMT cardiotoxicity by counteracting AMT's actions on the RyR2 channel complex.

Discussion

Our data demonstrate a novel mechanism of action for AMT: AMT activates the RyR2 SR Ca^{2+} release complex. Cardiac calsequestrin, also associated with the RyR2 complex and a putative AMT binding site, is not required for AMT action. AMT binds preferentially to open RyR2 channels, locking them in a subconductance state. The activation of RyR2 channels seems to be the main mechanism by which AMT causes SR Ca^{2+} leak, generates spontaneous SR Ca^{2+} release, and eventually depletes SR Ca^{2+} stores. Given that AMT activates the RyR2 SR Ca^{2+} release complex at concentrations that are commonly observed in patients taking AMT (Hardman and Limbird, 2001), the AMT action on RyR2 channels may contribute to the cardiotoxicity of AMT in patients.

Mechanisms of AMT Activation of RyR2 Channels. The action of AMT on cardiac RyR2s has marked similarities to that of ryanoids such as ryanodine, ryanodol (Tanna et al., 2000), and 21-amino-9α-hydroxy-ryanodine (Tanna et al., 1998). Both AMT and the ryanoids seem to bind to the channel only in its open state and induce long-lasting channel subconductance states. Moreover, AMT and ryanodine activate RyR2s at low concentrations, whereas at concentrations above 100 μM, both molecules inhibit them (Buck et al., 1992). The ryanodine binding site has been located in the 76-kDa region of RyR1 between amino acid position 4475 and the C terminus, a region that contains the putative channel pore (Callaway et al., 1994). The voltage-dependence of AMT binding also suggests a binding site in the trans-membrane C terminus of the RyR. However, in the case of ryanodols, comparative molecular field analysis of their effect on channel conductance suggests that they bind away from the ion-conducting pathway, probably in the channel vestibule (Welch et al., 1994). It is noteworthy that the X-ray crystal structure of the leucine transporter from *Aquifex aeolicus* has revealed a TCA binding site at the inner end of its extra cellular cavity (Zhou et al., 2007). This site is located within the membrane and binding of the TCA constrains the transmembrane α-helix 1 to prevent leucine release into the cytoplasm.

The mechanism for the voltage-dependence of AMT binding is not yet clear. Because AMT is cationic in aqueous solutions [pK_a = 9.2 (Deo et al., 2004)], it is possible that the voltage dependence stems from the voltage difference between the binding site and the luminal and cytoplasmic baths. However, according to the Woodhull model (Woodhull, 1973), RyR2 activation by luminal and cytoplasmic AMT

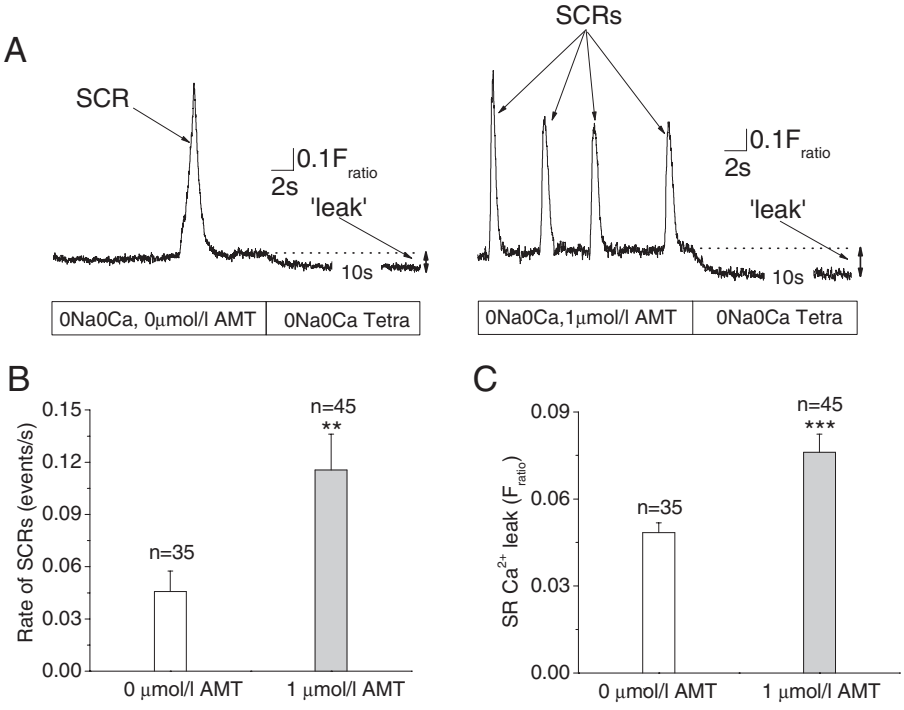

Fig. 10. AMT induces SCRs in absence of transsarcolemmal Ca^{2+} fluxes by increasing SR Ca^{2+} leak. A, representative examples of fluorescence records obtained from quiescent Fura-2-loaded myocytes exposed to 0 and 1 μM AMT (left and right, respectively) in Na^+- and Ca^{2+}-free Tyrode's solution, which abolishes transsarcolemmal Ca^{2+} flux. Note that SCRs were more frequent in the AMT-exposed myocyte. As indicated, external solution was then rapidly changed to Na^+- and Ca^{2+}-free Tyrode's solution containing 1 mM tetracaine, a blocker of RyR2 channels. The resulting drop in the fluorescence record (arrow) represents an estimate of diastolic SR Ca^{2+} leak (see *Materials and Methods* for details). Comparison of SCRs rates (B) and SR Ca^{2+} leak (C) in myocytes exposed to 0 and 1 μM AMT. Data represent the average number of SCRs per second during a recording period of 30 s for each myocyte. Note that 1 μM AMT significantly increased both the rate of SCRs and Ca^{2+} leak even when transsarcolemmal Ca^{2+} fluxes are eliminated. **, $p < 0.01$; ***, $p < 0.001$ using Student's t test.

should have opposite voltage dependencies because the transmembrane electric field will have opposite effects on the binding of AMT molecules originating from luminal and cytoplasmic baths. This prediction does not tally with our data in Fig. 4E, which shows that the slope of the voltage dependencies of cytoplasmic and luminal AMT binding are identical. A more likely explanation is that AMT binding is determined by the voltage-dependent properties of the AMT binding site and/or AMT molecule, such as has been proposed for ryanodine-related compounds (Tanna et al., 2000). Furthermore, the fact that cytoplasmic and luminal AMT induce identical RyR2 gating patterns with identical voltage-dependencies indicates that the same site/sites can be accessed by AMT molecules from both sides of the membrane. This hypothesis is consistent with the known partitioning of AMT into lipid bilayers (Deo et al., 2004) and the slow reversibility of AMT activation seen in Fig. 5.

Role of AMT Action on the RyR2 SR Ca^{2+} Release Complex in Myocardial Contractile Dysfunction and Sudden Cardiac Death. To date, both the proarrhythmic risk and myocardial contractile depression observed in AMT overdose have been primarily attributed to Na^+ channel block (Pimentel and Trommer, 1994; Thanacoody and Thomas, 2005). Nonetheless, mechanisms by which AMT decreases contractile function remain incompletely understood (Pimentel and Trommer, 1994). Factors other than sodium channel block have been implicated for direct myocardial contractile impairment in overdose situations (Knudsen and Abrahamsson, 1994). Thus, the heretofore unrecognized activating effect of AMT on the RyR2 complex may explain several aspects of AMT-induced cardiotoxicity: AMT causes spontaneous SR Ca^{2+}-release events (Fig. 9), which are known to cause delayed after-depolarizations and predispose to ventricular arrhythmias and sudden cardiac death (Wit and Rosen, 1983). Thus, the effect of AMT is akin to that of RyR2 and Casq2 mutations causing spontaneous SR Ca^{2+}-release events and ventricular arrhythmia in mice and humans (Knollmann and Roden, 2008). Furthermore, the SR Ca^{2+} depletion observed at AMT concentration as low as 500 nM in intact myocytes (Fig. 8, A and B) may cause myocardial contractile depression in overdose situations. AMT also inhibits the SR Ca^{2+} ATPase with a K_d of ~100 μM (Kim et al., 2005). SR Ca^{2+} ATPase inhibition could contribute to the profound SR Ca^{2+} depletion seen with very high concentrations of AMT (Fig. 8). It is also possible that AMT inhibits membrane proteins such as L-type Ca^{2+} channels and Na^+/Ca^{2+} exchanger at higher concentrations that would also deplete intracellular Ca^{2+}. However, these mechanisms are less likely to be relevant in vivo given that AMT concentrations in human plasma are $\leq$3 μM.

The activating effect of AMT on the RyR2 complex may not be a "class effect" in contrast to the Na^+ channel blockade seen with the TCAs. In a similar study, Watts et al. (1998) found no effect of imipramine (a related TCA) on the caffeine-induced Ca^{2+} transients at 30 μM. This hypothesis has to be tested in future studies

RyR2 channel dysfunction is emerging as a paradigm for both genetic and acquired human diseases (Knollmann and

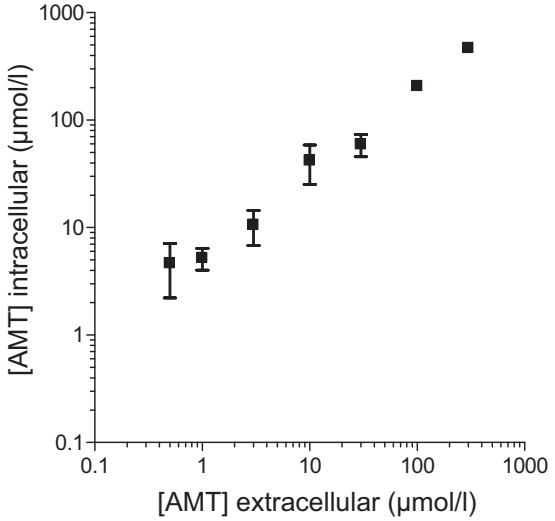

Fig. 11. AMT accumulates in myocytes leading to higher intracellular concentrations. Myocytes were incubated with AMT (0–300 μM) for 1 h and washed three times to remove extracellular AMT, and the amount of AMT retained intracellularly determined by LC/MS/MS after liquid phase extraction using imipramine as an internal standard (see *Materials and Methods* for details). Each point represents three separate experiments. Note that intracellular concentrations of AMT are approximately 5 times greater than that of the extracellular AMT concentrations in the bath, suggesting accumulation of AMT inside the cell.

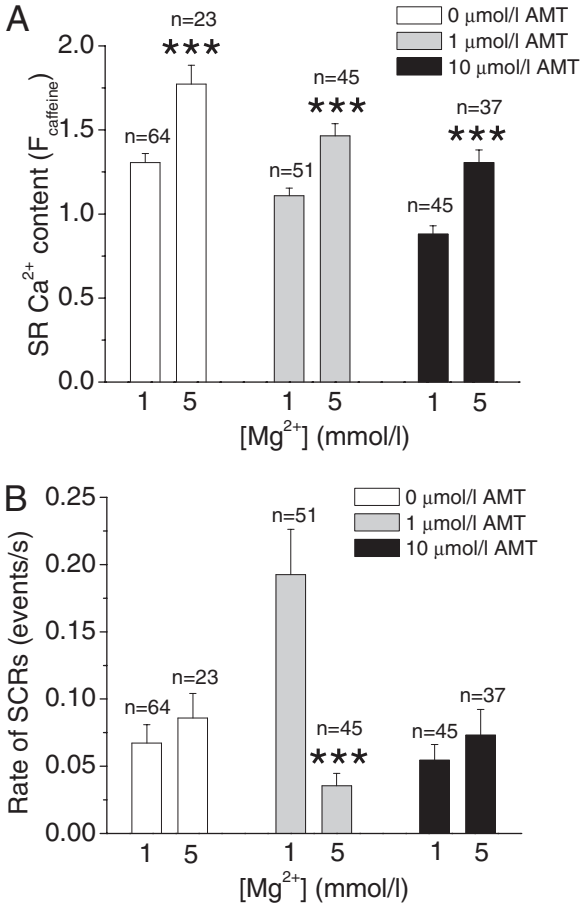

Fig. 12. Mg^{2+} restores SR Ca^{2+} content and prevents SCRs in AMT-exposed myocytes. A, average values of SR Ca^{2+} content in presence of low (1 mM) and high (5 mM) Mg^{2+} in myocytes exposed to 0, 1 and 10 μM AMT. B, incidence of SCRs in myocytes exposed to 0, 1, and 10 μM AMT in presence of low (1 mM) and high (5 mM) Mg^{2+}. Note that high Mg^{2+} (5 mM) completely abolished the AMT-induced increase in SCRs. This suggests that the stabilizing effect of Mg^{2+} on RyR2 channels preferentially antagonizes the action of AMT. **, $p < 0.01$; ***, $p < 0.001$ using Student's t test.

Roden, 2008). Although the intracellular RyR2 complex may not seem an obvious target for drug-related adverse effects, many drugs such as TCAs penetrate and accumulate inside myocytes (Walter and Gutknecht, 1986). Consistent with these reports, we demonstrate a 5-fold increase of intracellular compared with extracellular AMT concentrations. Analogous to drug-acquired channelopathies such as K^+ channel blockade causing QTc prolongation and *torsades de pointe*, AMT's activation of the RyR2 complex may serve as a paradigm for drug-related cardiotoxicity and should be considered whenever drug toxicity involves cardiomyopathy and ventricular arrhythmias without overt QTc prolongation.

RyR2 Channel Complex As a Therapeutic Target in AMT Cardiotoxicity. The RyR2 channel complex may represent a target to prevent or treat AMT-induced cardiotoxicity. We show that Mg^{2+} blocks the direct activating effect of AMT on the RyR2 complex in both bilayers and intact myocytes. Mg^{2+} is known to inhibit the RyR2 channel by at least 2 different mechanisms (Laver et al., 1997). Because AMT binds to RyR2 channel in open state, presence of high Mg^{2+} can be predicted to attenuate the effect of AMT on the RyR2 complex. Consistent with this idea, we show that high Mg^{2+} prevented the AMT induced spontaneous Ca^{2+} release events in intact myocytes (Fig. 12), which suggests that the effect of Mg^{2+} may be relevant in the intact cardiac muscle. This mechanism may partly explain the therapeutic efficacy of Mg^{2+} in the treatment of AMT cardiotoxicity in both humans (Citak et al., 2002) and rats (Knudsen and Abrahamsson, 1994).

Conclusion

AMT activates SR Ca^{2+} release by acting on the RyR2 channel itself, or associated proteins that are known to influence Ca^{2+} release. Also its action may be counteracted by increasing Mg^{2+}. Taken together, our results identify a novel mechanism of AMT action and suggest a potential therapeutic approach for the treatment of AMT-induced cardiotoxicity.

Acknowledgments

We are grateful to Karl Pfeifer, National Institutes of Health, for invaluable help generating the Casq2 mouse model, and Katherine Bradley and Paul Johnson for assisting with the bilayer experiments.

References

Buck E, Zimanyi I, Abramson JJ, and Pessah IN (1992) Ryanodine stabilizes multiple conformational states of the skeletal muscle calcium release channel. *J Biol Chem* **267:**23560–23567.

Callaway C, Seryshev A, Wang JP, Slavik KJ, Needleman DH, Cantu C 3rd, Wu Y, Jayaraman T, Marks AR, and Hamilton SL (1994) Localization of the high and low affinity [3H]ryanodine binding sites on the skeletal muscle Ca^{2+} release channel. *J Biol Chem* **269:**15876–15884.

Chopra N, Kannankeril PJ, Yang T, Hlaing T, Holinstat I, Ettensohn K, Pfeifer K, Akin B, Jones LR, Franzini-Armstrong C, et al. (2007) Modest reductions of cardiac calsequestrin increase sarcoplasmic reticulum Ca^{2+} leak independent of luminal Ca^{2+} and trigger ventricular arrhythmias in mice. *Circ Res* **101:**617–626.

Citak A, Soysal DD, Uçsel R, Karaböcüoğlu M, and Uzel N (2002) Efficacy of long duration resuscitation and magnesium sulphate treatment in amitriptyline poisoning. *Eur J Emerg Med* **9:**63–66.

Crouch BI, Caravati EM, Mitchell A, and Martin AC (2004) $P_o$isoning in older adults: a 5-year experience of US poison control centers. *Ann Pharmacother* **38:**2005–2011.

Deo N, Somasundaran T, and Somasundaran P (2004) Solution properties of amitriptyline and its partitioning into lipid bilayers. *Colloids Surf B Biointerfaces* **34:**155–159.

Györke S, Györke I, Lukyanenko V, Terentyev D, Viatchenko-Karpinski S, and Wiesner TF (2002) Regulation of sarcoplasmic reticulum calcium release by luminal calcium in cardiac muscle. *Front Biosci* **7:**d1454–1463.

Hardman JG and Limbird LE (2001) *Goodman and Gilman's The Pharmacological Basis of Therapeutics*, The McGraw-Hill Companies, Inc., New York.

Heard K, Cain BS, Dart RC, and Cairns CB (2001) Tricyclic antidepressants directly depress human myocardial mechanical function independent of effects on the conduction system. *Acad Emerg Med* **8:**1122–1127.

Kim E, Tam M, Siems WF, and Kang C (2005) Effects of drugs with muscle-related side effects and affinity for calsequestrin on the calcium regulatory function of sarcoplasmic reticulum microsomes. *Mol Pharmacol* **68:**1708–1715.

Knollmann BC, Chopra N, Hlaing T, Akin B, Yang T, Ettensohn K, Knollmann BE, Horton KD, Weissman NJ, Holinstat I, et al. (2006) Casq2 deletion causes sarcoplasmic reticulum volume increase, premature Ca release, and catecholaminergic polymorphic ventricular tachycardia. *J Clin Invest* **116:**2510–2520.

Knollmann BC and Roden DM (2008) A genetic framework for improving arrhythmia therapy. *Nature* **451:**929–936.

Knudsen K and Abrahamsson J (1994) Effects of epinephrine, norepinephrine, magnesium sulfate, and milrinone on survival and the occurrence of arrhythmias in amitriptyline poisoning in the rat. *Crit Care Med* **22:**1851–1855.

Laver DR, Baynes TM, and Dulhunty AF (1997) Magnesium inhibition of ryanodine-receptor calcium channels: evidence for two independent mechanisms. *J Membr Biol* **156:**213–229.

Laver DR and Curtis BA (1996) Response of ryanodine receptor channels to Ca^{2+} steps produced by rapid solution exchange. *Biophys J* **71:**732–741.

Laver DR, Roden LD, Ahern GP, Eager KR, Junankar PR, and Dulhunty AF (1995) Cytoplasmic Ca^{2+} inhibits the ryanodine receptor from cardiac muscle. *J Membr Biol* **147:**7–22.

Park IY, Kim EJ, Park H, Fields K, Dunker AK, and Kang C (2005) Interaction between cardiac calsequestrin and drugs with known cardiotoxicity. *Mol Pharmacol* **67:**97–104.

Pimentel L and Trommer L (1994) Cyclic antidepressant overdoses. A review. *Emerg Med Clin North Am* **12:**533–547.

Ray WA, Meredith S, Thapa PB, Hall K, and Murray KT (2004) Cyclic antidepressants and the risk of sudden cardiac death. *Clin Pharmacol Ther* **75:**234–241.

Shannon TR, Ginsburg KS, and Bers DM (2002) Quantitative assessment of the SR Ca^{2+} leak_load relationship. *Circ Res* **91:**594–600.

Sigworth FJ and Sine SM (1987) Data transformations for improved display and fitting of single-channel dwell time histograms. *Biophys J* **52:**1047–1054.

Tanna B, Welch W, Ruest L, Sutko JL, and Williams AJ (1998) Interactions of a reversible ryanoid (21-amino-9alpha-hydroxy-ryanodine) with single sheep cardiac ryanodine receptor channels. *J Gen Physiol* **112:**55–69.

Tanna B, Welch W, Ruest L, Sutko JL, and Williams AJ (2000) The interaction of a neutral ryanoid with the ryanodine receptor channel provides insights into the mechanisms by which ryanoid binding is modulated by voltage. *J Gen Physiol* **116:**1–9.

Thanacoody HK and Thomas SH (2005) Tricyclic antidepressant poisoning: cardiovascular toxicity. *Toxicol Rev* **24:**205–214.

Venetucci LA, Trafford AW, and Eisner DA (2007) Increasing ryanodine receptor open probability alone does not produce arrhythmogenic calcium waves: threshold sarcoplasmic reticulum calcium content is required. *Circ Res* **100:**105–111.

Vieweg WV and Wood MA (2004) Tricyclic antidepressants, QT interval prolongation, and torsade de pointes. *Psychosomatics* **45:**371–377.

Walter A and Gutknecht J (1986) Permeability of small nonelectrolytes through lipid bilayer membranes. *J Membr Biol* **90:**207–217.

Watts JA, Yates KM, Badar SK, Marcengill MB, and Kline JA (1998) Mechanisms of Ca^{2+} antagonism in imipramine-induced toxicity of isolated adult rat cardiomyocytes. *Toxicol Appl Pharmacol* **153:**95–101.

Welch W, Ahmad S, Airey JA, Gerzon K, Humerickhouse RA, Besch HR Jr, Ruest L, Deslongchamps P, and Sutko JL (1994) Structural determinants of high-affinity binding of ryanoids to the vertebrate skeletal muscle ryanodine receptor: a comparative molecular field analysis. *Biochemistry* **33:**6074–6085.

Wit AL and Rosen MR (1983) Pathophysiologic mechanisms of cardiac arrhythmias. *Am Heart J* **106:**798–811.

Woodhull AM (1973) Ionic blockage of sodium channels in nerve. *J Gen Physiol* **61:**687–708.

Zahradníková A, Dura M, and Györke S (1999) Modal gating transitions in cardiac ryanodine receptors during increases of Ca^{2+} concentration produced by photolysis of caged Ca^{2+}. *Pflugers Arch* **438:**283–288.

Zhou Z, Zhen J, Karpowich NK, Goetz RM, Law CJ, Reith ME, and Wang DN (2007) LeuT-desipramine structure reveals how antidepressants block neurotransmitter reuptake. *Science* **317:**1390–1393.

Address correspondence to: Dr. Björn C. Knollmann, Oates Institute for Experimental Therapeutics, Division of Clinical Pharmacology, Vanderbilt University Medical Center, 1265 Medical Research Building IV, Nashville, TN 37232-0575. E-mail: bjorn.knollmann@vanderbilt.edu